


Quadrupole stability in nonuniform fill patterns

F. J. Cullinan,^{*} Å. Andersson, and P. F. Tavares
 MAX IV Laboratory, Lund University, SE-22100 Lund, Sweden

 (Received 8 November 2021; accepted 30 March 2022; published 18 April 2022)

In previous publications, the effect of inhomogeneous beam loading of Landau cavities due to a nonuniform fill pattern in a storage ring has been studied with the aim of predicting the resulting longitudinal profiles of the bunches and their time offsets relative to the main rf [T. Olsson *et al.*, *Phys. Rev. Accel. Beams* **21**, 120701 (2018)]. This work was extended to treat dipolar coupled-bunch modes driven by beam-excited higher-order modes in the rf cavities [F. J. Cullinan *et al.*, *Phys. Rev. Accel. Beams* **23**, 074402 (2020)]. These coupled-bunch modes are of interest because they can become unstable, leading to an increase in the energy spread. The theory has now been extended once again to cover the case of coupled-bunch quadrupole modes where it is the lengths of the bunches that are oscillating, not their centroids. The theory is outlined and its predictions are thoroughly benchmarked against predictions from macroparticle tracking. Observations of the effects of nonuniform fill patterns on coupled-bunch quadrupole instabilities are made and interpreted. Results of measurements at the MAX IV 3 GeV ring, interpreted using theoretical calculations, are then presented to continue the investigation.

DOI: [10.1103/PhysRevAccelBeams.25.044401](https://doi.org/10.1103/PhysRevAccelBeams.25.044401)

I. INTRODUCTION

In a previous publication [1], the stability of coupled-bunch modes driven by higher order modes (HOMs) in the rf cavities was investigated for the case of a bunched beam in a storage ring and specifically, for cases where the fill pattern of the ring is nonuniform. This work was an extension of a previous investigation [2] into how the inhomogeneous¹ beam loading of the cavities that arises due to such fill patterns leads to slippage in the phase of the different bunches relative to the rf wave. This paper extends the work once again to also account for coupled-bunch quadrupole instabilities: oscillations of the bunch length. As before, the theory developed takes into account the variation in the time intervals between consecutive bunches and the Landau damping due to the tune spread between bunches (interbunch) but it does not account for the tune spread within each bunch (intrabunch).

As is the case with their dipolar counterparts, coupled-bunch quadrupole instabilities typically result in a

significant increase in the energy spread which, in the case of synchrotron light sources, degrades the brilliance of the light delivered to the beamlines. As an additional motivation, quadrupole instabilities cannot be effectively damped using the most common type of longitudinal bunch-by-bunch feedback, which applies an energy kick that is uniform over the bunch length based on previous measurements of the phase or energy offset of the bunch centroid. Some damping has been demonstrated by exploiting bunch-length sensitivity in the centroid measurements and using a sinusoidal energy kick off crest but it is by no means optimized and comes at the cost of worse damping of dipole modes [4]. As a result, quadrupole instabilities can limit the maximum current that can be stored in rings that rely on a feedback for longitudinal stability [4,5].

In order to validate this latest extension of the theory, its predictions are benchmarked extensively against the results of macroparticle tracking carried out using MBTRACK [6]. Some important limitations and considerations are in this way identified. The effects of the nonuniform fill on a quadrupole instability are investigated for the case of the MAX IV 3 GeV ring. The use of Landau cavities, specifically in fourth generation storage-ring light sources, was a key motivation for the previous investigations as they have a large effect on the beam phase slippage when there is a nonuniform fill pattern. This is found to also be of importance here. As part of the investigation, measurements of a coupled-bunch quadrupole instability were made at the MAX IV 3 GeV ring for different fill patterns. The results are compared to predictions made using the theory.

^{*}francis.cullinan@maxiv.lu.se

¹The word “transient” has been used in place of the word “inhomogeneous” in previous publications but the latter is adopted here as a more accurate alternative as pointed out by Warnock and Venturini [3]. Similarly, the previously used phrase “beam phase transient” has been replaced with “beam phase slippage.”

Published by the American Physical Society under the terms of the Creative Commons Attribution 4.0 International license. Further distribution of this work must maintain attribution to the author(s) and the published article's title, journal citation, and DOI.

The outline of the rest of the paper is as follows. Section II outlines the theory. In Sec. III, the predictions of the theory are compared to predictions made using the macroparticle tracking code MBTRACK [6] and some general observations of the behavior of coupled-bunch quadrupole modes in the presence of a nonuniform fill are made. Section IV presents a continuation of the investigation with the results of measurements made at the MAX IV 3 GeV ring, which the theory is used to interpret. Finally, the main conclusions are summarized in Sec. V.

II. THEORY

The approach followed here is the one taken by Lindberg [7]. An expression for the wake potential is derived and this is then used to construct a Hamiltonian for the motion of particles within a bunch. The Hamiltonian is, in turn, substituted into the Vlasov equation. The coordinate system used here in longitudinal phase space is a normalized energy offset $\delta = \Delta E/E_0$ and a time offset τ from the equilibrium time offset ζ at which a particle receives no net energy gain per turn [2]. The purpose of defining an equilibrium time offset is to allow it to vary between bunches. This time offset is relative to a chosen arbitrary phase of the main rf wave and a positive value for τ or ζ is earlier in time in contrast to the arrival time t where a larger value is later. Using this notation, the wake potential V_{wake} at bunch n due to the wakefield from bunch j summed over infinite previous turns is given by

$$V_{\text{wake},j}(\tau, t) = -\frac{eI_j}{E_0} \int d\hat{\tau} d\hat{\delta} \sum_{l=0}^{\infty} \Psi_j(\hat{\tau}, \hat{\delta}, t - lT_0) \times \int^{\tau} d\tau' W_{\parallel}[\hat{\tau} + \Delta t(\zeta_n, \zeta_j) + lT_0 - \tau'] \quad (1)$$

where Ψ is the normalized distribution of particles in longitudinal phase space, W_{\parallel} is the longitudinal wake function, I_j is the current of bunch j , E_0 is the beam energy, e is the elementary charge, T_0 is the revolution period of the machine, c is the speed of light in vacuum and Δt is the difference in arrival time between the two bunches as defined in [1] as

$$\Delta t(\zeta_n, \zeta_j) = \begin{cases} \zeta_j - \zeta_n + (n - j + h)/f_{\text{rf}} & \text{for } n \leq j \\ \zeta_j - \zeta_n + (n - j)/f_{\text{rf}} & \text{for } n > j \end{cases} \quad (2)$$

where f_{rf} is the frequency of the main rf and h is the harmonic number of the ring. The bunch distribution is expanded into a fixed distribution $\Psi_{0,j}$ plus a perturbation ψ_j that varies in time and contains no net charge:

$$\Psi_j(\tau, \delta, t) = \Psi_{0,j}(\tau, \delta) + \psi_j(\tau, \delta, t) \quad (3)$$

$$\int \psi_j(\hat{\tau}, \hat{\delta}, t - lT_0) d\hat{\tau} d\hat{\delta} = 0. \quad (4)$$

The next step is to perform a Taylor expansion of the integrated wake function, keeping in mind that, because we want to evaluate the quadrupole instability, we are interested in the second-order moment of the bunch and so will only be keeping terms of second order in $\hat{\tau}$. For reasons that will come apparent later, we must continue the Taylor expansion up to third order.

$$\begin{aligned} & \int^{\tau} d\tau' W_{\parallel}[\hat{\tau} + \Delta t(\zeta_n, \zeta_j) + lT_0 - \tau'] \\ & \approx \int^{\tau} d\tau' \left\{ W_{\parallel}(\xi) + (\hat{\tau} - \tau') \frac{dW_{\parallel}}{d\xi} \right. \\ & \quad + \frac{1}{2!} (\hat{\tau} - \tau')^2 \frac{d^2 W_{\parallel}}{d\xi^2} + \frac{1}{3!} (\hat{\tau} - \tau')^3 \frac{d^3 W_{\parallel}}{d\xi^3} \\ & \quad \left. + \mathcal{O}[(\hat{\tau} - \tau')^4] \right\}_{\xi=\Delta t(\zeta_n, \zeta_j)+lT_0}. \end{aligned} \quad (5)$$

Doing this restricts the theory to wake functions that vary slowly over the passage of the bunch. This is the case for most cavity HOMs in electron storage rings, for example, whose periods of oscillation tend to be much longer than the bunch duration. Evaluating the integral, expanding and neglecting all terms except for those that contain $\hat{\tau}^2$ leaves

$$\left(\frac{\hat{\tau}^2 \tau}{2} \frac{d^2 W_{\parallel}}{d\xi^2} - \frac{\hat{\tau}^2 \tau^2}{4} \frac{d^3 W_{\parallel}}{d\xi^3} \right)_{\xi=\Delta t(\zeta_n, \zeta_j)+lT_0}. \quad (6)$$

Doing this is justified for the following reasons. First, constant-wake terms are neglected. These affect the equilibrium time offset of the bunch due to the additional energy loss. They also affect the synchrotron oscillation frequency due to the change in the slope of the rf voltage. If desired, these effects can be included in the matrix method outlined in [2] or it can simply be assumed that they are small compared to other constant-wake sources, as in [1]. Second, it is assumed that the bunch has no dipole moment so first order terms in $\hat{\tau}$ are left out. Third, the perturbation has been defined as containing no net charge. The wake potential is then written as

$$V_{\text{wake},j}(\tau; t) = -\frac{eI_j}{E_0} \sum_{l=0}^{\infty} \left[\frac{\tau}{2} \frac{d^2 W_{\parallel}}{d\xi^2} - \frac{\tau^2}{4} \frac{d^3 W_{\parallel}}{d\xi^3} \right]_{\xi=\Delta t(\zeta_n, \zeta_j)+lT_0} \times \int \psi_j(\hat{\tau}, \hat{\delta}, t - lT_0) \hat{\tau}^2 d\hat{\tau} d\hat{\delta}. \quad (7)$$

The next step is completely analogous to what is done in [7]. Equation (7) is summed over all drive bunches (or, more accurately, over all rf buckets whether they contain any charge or not) and incorporated into a Hamiltonian for particle motion within the witness bunch. In action-angle coordinates (J, Φ) , the Hamiltonian is

$$H_n = H_{0,n}(J) + \sum_{j=0}^{h-1} V_{\text{wake},j}(\Phi, J) \quad (8)$$

where the wake potential has been converted to action-angle coordinates and the first term H_0 contains the rf potential and can also incorporate constant wake terms, as explained in [7]. The Vlasov equation in action-angle coordinates is

$$\frac{\partial \Psi_n}{\partial t} + \frac{\partial \Phi}{\partial t} \frac{\partial \Psi_n}{\partial \Phi} + \frac{\partial J}{\partial t} \frac{\partial \Psi_n}{\partial J} = \frac{\partial \Psi_n}{\partial t} + \frac{\partial H_n}{\partial J} \frac{\partial \Psi_n}{\partial \Phi} - \frac{\partial H_n}{\partial \Phi} \frac{\partial \Psi_n}{\partial J} = 0. \quad (9)$$

Substituting in the Hamiltonian and neglecting all terms of higher than first order in the perturbation ψ_n , remembering that the wake potential is itself first order, the Vlasov equation is linearized to

$$\frac{\partial \psi_n}{\partial t} + \omega_n(J) \frac{\partial \psi_n}{\partial \Phi} - \sum_{j=0}^{h-1} \frac{\partial V_{\text{wake},j}}{\partial \Phi} \frac{\partial \Psi_{0,n}}{\partial J} = 0 \quad (10)$$

where $\omega_n(J) = \partial \Phi / \partial t = \partial H_n / \partial J$ is the action-dependent incoherent synchrotron frequency which characterizes the rf potential for that bucket.

Converting Eq. (7) to action-angle coordinates, substituting it into Eq. (10) and performing the same manipulations as in [7], the linearized Vlasov equation becomes

$$\begin{aligned} & \tilde{\psi}_n(\Phi, J) e^{-i\Omega\Phi/\omega_n} [e^{-2\pi i\Omega/\omega_n} - 1] \\ &= \frac{\partial \Psi_{0,n}}{\partial J} \sum_{j=0}^{h-1} \frac{e I_j}{E_0} \langle \tau^2 \rangle_j \sum_{l=0}^{\infty} e^{il\Omega T_0} \frac{1}{\omega_n(J)} \\ & \times \int_{\Phi}^{\Phi+2\pi} d\Phi' e^{-i\Omega\Phi'/\omega_n} \left[\frac{1}{2} \frac{\partial \tau}{\partial \Phi'} \frac{d^2 W_{\parallel}}{d\xi^2} \right. \\ & \left. - \frac{1}{4} \frac{\partial(\tau^2)}{\partial \Phi'} \frac{d^3 W_{\parallel}}{d\xi^3} \right]_{\xi=\Delta t(\zeta_n, \zeta_j) + lT_0}. \end{aligned} \quad (11)$$

Equation (11) resembles Eq. (15) in [7], the only difference being the term in square brackets replacing derivatives of the longitudinal coordinate and the wake function. Here, Ω is the complex frequency of coherent oscillation and characterizes the assumed time evolution of the perturbation:

$$\psi_n(\Phi, J, t) = \tilde{\psi}_n(\Phi, J) e^{-i\Omega t}. \quad (12)$$

The amplitude of the quadrupole oscillation of bunch n is defined as the quadrupole moment

$$\langle \tau^2 \rangle_n = \int \hat{\tau}^2(\Phi, J) \tilde{\psi}_n(\Phi, J) d\Phi dJ. \quad (13)$$

Following on from this, the longitudinal coordinate is expanded as a Fourier series $\tau = \sum_m e^{im\Phi} \tau_m(J)$ so that, after performing the integration over Φ' , Eq. (11) becomes

$$\begin{aligned} \tilde{\psi}_n(\Phi, J) &= \frac{\partial \Psi_{0,n}}{\partial J} \sum_{j=0}^{h-1} \frac{e I_j}{E_0} \langle \tau^2 \rangle_j \sum_{l=0}^{\infty} e^{il\Omega T_0} \frac{1}{\omega_n(J)} \sum_m \left[\frac{m \tau_m(J) e^{im\Phi}}{2[m - \Omega/\omega_n(J)]} \frac{d^2 W_{\parallel}}{d\xi^2} \right. \\ & \left. - \sum_p \frac{(m+p) \tau_m(J) \tau_p(J) e^{i(m+p)\Phi}}{4[m+p - \Omega/\omega_n(J)]} \frac{d^3 W_{\parallel}}{d\xi^3} \right]_{\xi=\Delta t(\zeta_n, \zeta_j) + lT_0}. \end{aligned} \quad (14)$$

The next step is to multiply by τ^2 and integrate over all of phase space. Starting with the angle variable Φ , everything on the right-hand side outside the square brackets is independent and multiplying the terms inside the square brackets by τ^2 leaves the following integration:

$$\begin{aligned} & \int_0^{2\pi} d\Phi \tau^2 \sum_m \left[\frac{m \tau_m(J) e^{im\Phi}}{2[m - \Omega/\omega_n(J)]} \frac{d^2 W_{\parallel}}{d\xi^2} - \sum_p \frac{(m+p) \tau_m(J) \tau_p(J) e^{i(m+p)\Phi}}{4[m+p - \Omega/\omega_n(J)]} \frac{d^3 W_{\parallel}}{d\xi^3} \right]_{\xi=\Delta t(\zeta_n, \zeta_j) + lT_0} \\ &= \int_0^{2\pi} d\Phi \sum_{m,q,r} \left[\frac{m \tau_m(J) \tau_q(J) \tau_r(J) e^{i(m+q+r)\Phi}}{2[m - \Omega/\omega_n(J)]} \frac{d^2 W_{\parallel}}{d\xi^2} \right. \\ & \left. - \sum_p \frac{(m+p) \tau_m(J) \tau_p(J) \tau_q(J) \tau_r(J) e^{i(m+p+q+r)\Phi}}{4[m+p - \Omega/\omega_n(J)]} \frac{d^3 W_{\parallel}}{d\xi^3} \right]_{\xi=\Delta t(\zeta_n, \zeta_j) + lT_0}. \end{aligned} \quad (15)$$

To solve this, all orders of τ are excluded apart from $|m| = 1$, which is equivalent to assuming elliptical orbits for all particles in longitudinal phase space. We then see that the first term evaluates to zero because $m + q + r \neq 0$

for all combinations of $|m| = |q| = |r| = 1$. Additionally, the second term is only nonzero when $m = p \neq q = r$. The third-order term in the Taylor expansion of the wake function is the lowest-order term that drives the quadrupole

instability. This is intuitive since the first-order term is insensitive to the quadrupole moment while the second-order term is an equivalent kick to the head and the tail, not affecting the length of a symmetric bunch. Equation (14) thereby simplifies to

$$\begin{aligned} \langle \tau^2 \rangle_n &= \frac{4\pi e}{E_0} \sum_{j=0}^{h-1} I_j \langle \tau^2 \rangle_j \sum_{l=0}^{\infty} e^{il\Omega T_0} \\ &\times \int_0^{\infty} dJ \frac{1}{\omega_n(J)} \frac{\partial \Psi_{0,n}}{\partial J} \frac{|\tau_1(J)|^4}{\Omega^2/\omega_n^2(J) - 4} \\ &\times \left. \frac{d^3 W_{\parallel}}{d\xi^3} \right|_{\xi=\Delta t(\zeta_n, \zeta_j) + lT_0}. \end{aligned} \quad (16)$$

The derivation up to this point answers the challenge laid down by Lindberg to extend his analysis to moments of the bunch distribution that are of higher order than dipole [7]. The approximation of elliptical orbits was introduced a little earlier in order to complete the integration in Eq. (15) but this is not an overly restrictive approximation and is made later in [7] for all specific cases that are explored. One may then wish to perform the last step of evaluating Eq. (16) for specific rf potentials such as weakly anharmonic or quartic or alternatively, attempt to evaluate it numerically in a similar approach to that of Venturini [8]. The interest here, however, is to focus on nonuniform fill patterns.

For the integration over J , we assume a quadratic potential so that the distribution Ψ_n is Gaussian in both energy and time offset and ω_n is independent of J so there is no intrabunch Landau damping. The latter assumption was also made in [1] and was found to be justified for the nonuniform fill pattern studied. The following relations, also found in [7], then apply

$$\Psi_{0,n}(J) = \frac{e^{-J/(J)_n}}{2\pi \langle J \rangle_n} \quad (17)$$

$$\tau_1(J) = \tau_{-1}(J) = \sigma_{\tau,n} \sqrt{\frac{J}{2\langle J \rangle_n}} \quad (18)$$

$$\langle J \rangle_n = \sigma_{\tau,n} \sigma_{\delta,n} \quad (19)$$

$$\tau = \frac{\alpha_c}{\omega_n} \delta. \quad (20)$$

The differentiation with respect to and integration over J can then be evaluated analytically to give

$$\int_0^{\infty} \frac{\partial \Psi_{0,n}}{\partial J} |\tau_1|^4 dJ = -\frac{\sigma_{\tau,n}^3}{4\pi\sigma_{\delta,n}} = -\frac{\alpha_c \sigma_{\tau,n}^2}{4\pi\omega_n}. \quad (21)$$

Inserting this into Eq. (16) and rearranging the $\Omega^2 - 4\omega_n^2$ in the resulting denominator gives the eigenvalue equation

$$\begin{aligned} \Omega^2 \langle \tau^2 \rangle_n &= \sum_{j=0}^{h-1} \left[-\frac{e\alpha_c \sigma_{\tau,n}^2}{E_0} I_j \sum_{l=0}^{\infty} e^{il\Omega T_0} \frac{d^3 W_{\parallel}}{d\xi^3} + 4\omega_n^2 \delta_{nj} \right]_{\xi=\Delta t(\zeta_n, \zeta_j) + lT_0} \\ &\times \langle \tau^2 \rangle_j \end{aligned} \quad (22)$$

where δ_{nj} is the Kronecker delta.

Finally, we assume a resonant wakefield so that we can make the following substitution, similarly to in [2]:

$$\begin{aligned} \sum_{l=0}^{\infty} e^{il\Omega T_0} \left. \frac{d^3 W_{\parallel}}{d\xi^3} \right|_{\xi=\Delta t(\zeta_n, \zeta_j) + lT_0} &= -\frac{\omega_r R_L}{2Q_L} \left[\frac{(i\omega_r - \alpha)^3 e^{(i\omega_r - \alpha)\Delta t(\zeta_n, \zeta_j)}}{1 - e^{(i\omega_r - \alpha + i\Omega)T_0}} \right. \\ &\left. + \frac{(-i\omega_r - \alpha)^3 e^{(-i\omega_r - \alpha)\Delta t(\zeta_n, \zeta_j)}}{1 - e^{(-i\omega_r - \alpha + i\Omega)T_0}} \right], \end{aligned} \quad (23)$$

where ω_r is the resonant frequency of the resonator wake source and R_L and Q_L are the loaded shunt impedance and quality factor respectively. $\alpha = \omega_r/2/Q_L$ is the damping constant. Substituting Eq. (23) into Eq. (22) and solving for the eigenvalues in order to determine Ω allows for the prediction of the coherent frequency and growth rates of different coupled-bunch quadrupole modes driven by HOMs.

For the specific case of resonant wakefields, the accuracy can further be improved by introducing form factors to account for the variation of the wake function over the length of the bunch. Instead of Eq. (23), the following expression would then be substituted into Eq. (22) in the same place:

$$\begin{aligned} &-\frac{\omega_r R_L |F_j| |F_n|}{2Q_L} \\ &\times \left[\frac{(i\omega_r - \alpha)^3 e^{(i\omega_r - \alpha)\Delta t(\zeta_n, \zeta_j) + i(\varphi_j - \varphi_n)}}{1 - e^{(i\omega_r - \alpha + i\Omega)T_0}} \right. \\ &\left. + \frac{(-i\omega_r - \alpha)^3 e^{(-i\omega_r - \alpha)\Delta t(\zeta_n, \zeta_j) - i(\varphi_j - \varphi_n)}}{1 - e^{(-i\omega_r - \alpha + i\Omega)T_0}} \right]. \end{aligned} \quad (24)$$

where $F_j = |F_j| \exp(i\varphi_j)$ is the complex form factor of bunch j as defined in [2]. This restores some of the accuracy lost in the Taylor expansion in Eq. (6) but is only applicable to resonant wakefields so there is some loss of generality. Maintaining the assumptions of Gaussian bunches, $F_j F_n^* = \exp(-\omega_r^2(\sigma_{\tau,j}^2 + \sigma_{\tau,n}^2)/2)$.

Encouragingly, for uniform fill patterns and the zeroth order coupled-bunch mode where $\langle \tau^2 \rangle_j = \langle \tau^2 \rangle_n$, substituting Eq. (24) into Eq. (22) returns something similar to Eq. (13) in [9]. Furthermore, the same derivation was also carried out for the dipole moment and the result is equivalent to Eq. (14) in [1] if Gaussian bunches are assumed. This derivation is not outlined here since it is even

more similar to the one in [7], only differing in the last steps where the generality to arbitrary fill patterns is maintained. A method for evaluating quadrupole coupled-bunch instabilities analytically that is generalized to arbitrary fill patterns has therefore been successfully developed.

III. BENCHMARKING

The theory described in Sec. II has been benchmarked against the results of macroparticle tracking. Similarly to [1], the theory was used to calculate threshold shunt impedances of a specific HOM. That is, the shunt impedance at which the growth rate of the least stable coupled-bunch quadrupole mode is equal to the rate of damping due to synchrotron radiation. This is twice the radiation damping rate of the dipole modes as discussed in detail in [10] and essentially because the equations predict the evolution of moments of second order $\langle \tau^2 \rangle_n$. Above the threshold shunt impedance, a coupled-bunch quadrupole instability is predicted to develop. The predictions are compared with the results of HOM shunt-impedance scans in macroparticle tracking. The parameters used are those of the MAX IV 3 GeV ring, listed in Table I, which is identical to the table in [1] except here, the parameters of a HOM have been added. This HOM, later referred to as the “example HOM,” is 94.9 MHz above the tenth harmonic of the rf frequency so that it drives coupled-bunch mode number 167 in a uniform fill. Following convention, the damping time \mathcal{T}_0 (inverse of the damping rate) listed in Table I is the dipole-mode damping time.

It was found that the threshold shunt impedances for quadrupole instabilities were a lot higher than for a dipole instability driven by the same HOM. The calculation was performed for different fill patterns and different Landau-cavity voltages. A two-step method is used, similar to in [1]

TABLE I. Parameters of the MAX IV 3 GeV ring used for this study.

Parameter	Value
Energy E_0	3 GeV
Circumference	528 m
rf frequency f_{rf}	99.931 MHz
rf voltage V_0	1.251 MV
Beam current	250 mA
Harmonic number h	176
Energy loss per turn U_0	363.8 keV
Radiation damping time \mathcal{T}_0	25.194 ms
Momentum compaction α_c	0.000306
Natural normalized energy spread	0.000769
Landau cavity (LC) harmonic	3
Total LC shunt impedance $R_s = V^2/(2P)$	8.25 M Ω
LC quality factor	20800
HOM frequency on resonance	1094.13 MHz
HOM quality factor	24000
HOM shunt impedance	200 k Ω

where, in the first step, the phase slippage and bunch lengths are calculated using the matrix method introduced in [2] and in the second step, the stability of the stationary distribution against quadrupolar perturbations is determined. As in [1], the incoherent synchrotron frequency ω_n was calculated from the gradient of the total rf voltage using Eq. (17) in [2].

Because of the interplay between the tune shift and growth rates discussed in [1], an iterative minimization algorithm was used to arrive at a value for the threshold shunt impedance. For nonuniform fill patterns, the phase slippage had to be recalculated every iteration taking into account the beam loading of the HOM, which can have a significant impact. Figure 1 illustrates this effect and shows why such an approach is necessary. This was not done for the dipole coupled-bunch instabilities studied in [1] but may have been necessary if cases with lower Landau-cavity voltages had been studied, as discussed below.

The macroparticle tracking was performed using MBTRACK and the parameters listed in Table I. The simulations whose results are presented in this section include radiation damping and are of 40,000 turns of the MAX IV 3 GeV ring starting from the stable beam phase slippage expected in the absence of the HOM as generated using MBTRACK. A bunch-by-bunch feedback is included to suppress the dipole instability. This feedback employs energy detection and applies an energy kick to each bunch equal to its energy offset multiplied by a gain of -0.4 . In Figs. 2–4, the results of the simulations are shown in two-dimensional grids where each row is for a different HOM shunt impedance and each column, the value of some other parameter. The color of each grid cell represents the RMS bunch-length variation over the last 20,000 turns of the simulation. The first 20,000 turns are excluded in order to properly account for the change of the phase slippage due to the inhomogeneous beam loading of the HOM. For each scan of the shunt impedance, the minimum value for which simulations are performed is one that results in a stable

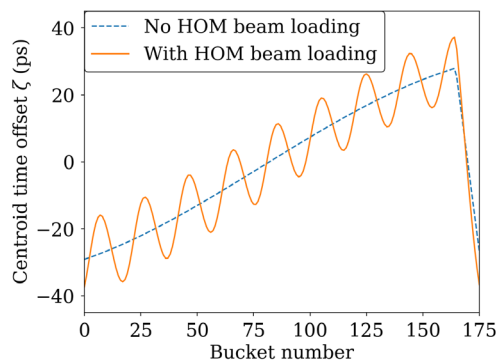


FIG. 1. Bunch-centroid time offsets with beam loading of the HOM at the threshold shunt impedance of the quadrupole instability compared to the case with no HOM beam loading at all. The results are for a case where 165 out of 176 rf buckets are filled and the Landau cavities are detuned by +150 kHz.

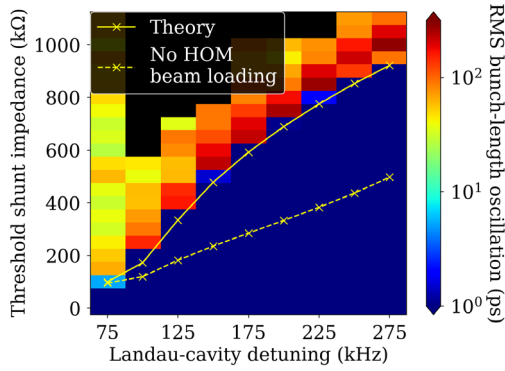


FIG. 2. RMS oscillation of the bunch length during macroparticle simulations indicating the stability of a HOM-driven coupled-bunch quadrupole instability compared to theoretical predictions of the threshold shunt impedance against the detuning of the Landau cavities. Black indicates that no simulation was run.

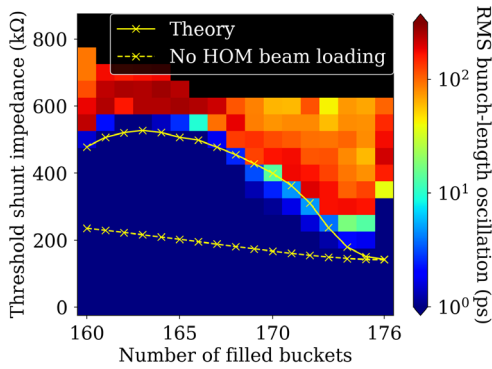


FIG. 3. Threshold shunt impedances above which a HOM-driven coupled-bunch quadrupole instability develops for different numbers of filled rf buckets as determined by theory compared to the bunch length stability observed in macroparticle tracking shown on a color scale where black indicates that no simulation was run.

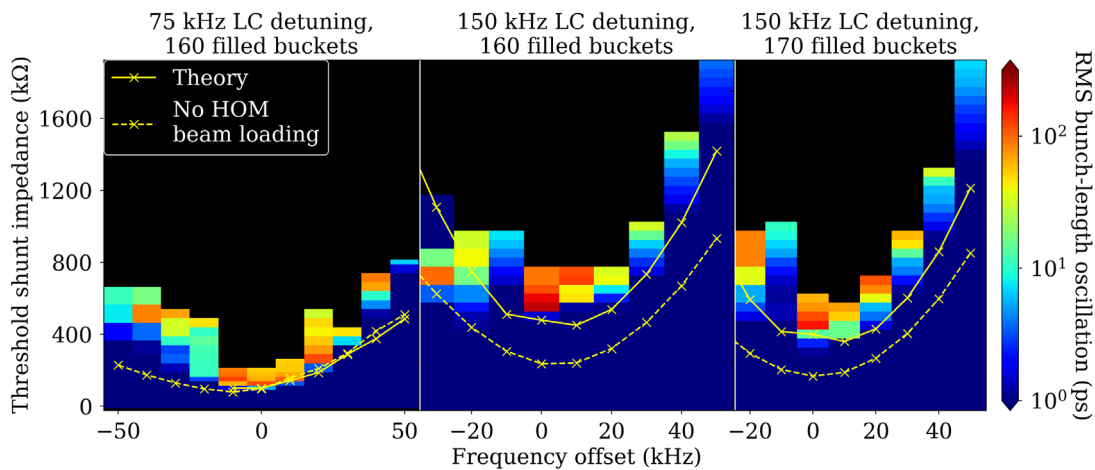


FIG. 4. Threshold shunt impedances above which a HOM-driven coupled-bunch quadrupole instability develops as determined by theory compared to the bunch length stability observed in macroparticle tracking shown on a color scale for different HOM frequencies and for three cases: a Landau-cavity detuning of 75 kHz and a 160 buckets filled (left), the same fill with a Landau-cavity detuning of 150 kHz (center) and a 150 kHz detuning with 165 buckets filled (right). Black indicates that no simulation was run.

beam. In the plots, the bunch length oscillation amplitude is assumed to be equal or lower for shunt impedances below those minimum values. No similar assumption is made for shunt impedances above threshold so points for which no simulation has been run are simply colored black.

A. Landau-cavity detuning

The influence of the Landau cavities was immediately checked because, as they greatly affect the phase slippage, it is likely to be large. Results are shown in Fig. 2 for the example HOM on resonance and a fill pattern where 160 rf buckets out of 176 are filled with equally charged bunches. The Landau cavity detuning has been varied between +75 kHz and +275 kHz. With a uniform fill, the former would result in a total Landau-cavity voltage of 381 kV, only slightly lower than the 396 kV that would be required to fully flatten the first derivative of the rf voltage, and +275 kHz is close to half the revolution frequency, which is practically the most a passive Landau cavity can be detuned to minimize its influence on the phase slippage.

The general trend is that the larger the Landau-cavity detuning (and thereby, the lower the Landau-cavity voltage), the larger the threshold shunt impedance. This was also seen in [1] and can be attributed to the reduction of the incoherent synchrotron frequency by the flattening of the rf potential (before any increase in the tune spread between bunches reverses the trend). This trend is further amplified by the effect of the HOM on the beam phase slippage, as can be seen in the difference between the results of the theoretical calculation with and without beam loading of the HOM. The Landau cavities have a smaller influence on the beam phase slippage as they are further detuned and so the HOM becomes more dominant. The HOM then becomes both the driver of the instability and the dominant source of the interbunch tune spread and this only increases

the threshold shunt impedance. On the other hand, at the smallest Landau detuning of 75 kHz, the beam-loading of the Landau cavities is large and is the dominant driver of the beam phase slippage. Consequently, the difference between the results with and without HOM beam loading is too small to be visible on the figure.

Effects included in the macroparticle tracking that are not included in the theory include the diffusion effects of quantum excitation and Landau damping due to intrabunch synchrotron tune spread. Nevertheless, there is a good level of agreement between tracking and the theory over the full detuning range.

B. Fill pattern

Keeping the HOM at its resonant frequency, the investigation was continued to see what happens when the fill pattern is varied. A midrange Landau cavity detuning of 150 kHz was chosen for the scan in fill pattern. Another value could just as well have been chosen. However, cases with moderate detuning are important because bunch-by-bunch feedback systems tend to struggle when there is a large Landau-cavity voltage because of both the broad spread in synchrotron tune and the lower average incoherent tune [11]. Furthermore, if the fill pattern is not uniform and the Landau-cavity voltage is high, it will not be possible for the timing of the feedback to be optimum for all bunches simultaneously because of the phase slippage between them. This is particularly true for systems whose dynamic range is limited by the use of a local oscillator at a high rf harmonic for phase detection and/or the use of a high-frequency cavity kicker to apply energy kicks to the beam.

The fill pattern was scanned by varying the number of filled rf buckets from 160 out of 176 to all 176 (a uniform fill). In all cases, all bunches are in consecutive buckets (so that there is only one bunch train) and contain equal charge. The beam current is kept constant at 250 mA so the shorter the bunch train, the higher the charge stored in each bunch.

The results are shown in Fig. 3. The fill pattern has a significant effect on the threshold shunt impedance. The general trend is that the threshold shunt impedance increases as the number of filled buckets decreases (or the fill pattern becomes less uniform). This is because of the Landau damping that arises from the tune spread between the different buckets. If the HOM beam loading is not included, a monotonic increase of the threshold shunt impedance with decreasing number of bunches is predicted. When it is included, however, the threshold shunt impedance peaks at 163 filled buckets. This behavior is dependent on the coupled-bunch mode number as shown later in Sec. IV.

There is good agreement between the theoretical predictions and the results of the macroparticle tracking across almost all fill patterns. However, the theory appears to significantly underestimate the threshold shunt impedance for a uniform fill and the macroparticle tracking shows a

sharp drop in the threshold shunt impedance when one bunch is removed. A possible explanation for this is that for a uniform fill, there is no tune spread between the bunches and so it is the intrabunch tune spread, which is not included in the theory, that is the dominant source of Landau damping. This scenario may never show up in practice because there will always be some interbunch tune spread due to random charge variation between the different bunches.

C. HOM detuning

Next, the theory was used to predict the threshold shunt impedances as the resonant frequency of the HOM was varied. This was done for a few Landau-cavity detunings and fill patterns and the results for three separate cases are shown in Fig. 4. In general, the agreement between theory and macroparticle tracking is good when the HOM is on resonance and when the HOM is detuned to higher frequency. However, the agreement is not so good when the HOM is detuned to lower frequency. This is because the coupled-bunch quadrupole mode is then shifted to very low frequency so that one period of coherent oscillation becomes comparable to the radiation damping time. This can have a large effect on the results of the theory if, as is the case here, the damping is not included in the calculation.

For some cases, the theory does not converge on a solution and so no result is shown for the case with HOM beam loading included. This does not mean that a solution does not exist. Rather, the beam-loading of the HOM becomes so large that the slope of the total voltage at the equilibrium time offset of some bunches switches sign. The bunches then effectively become overstretched and the theory is no longer valid. Otherwise, the change in threshold shunt impedance caused by including the beam loading of the HOM appears to be the same across the full tuning range.

For the Landau-cavity detuning of 150 kHz, when the HOM is detuned by -30 kHz, the macroparticle simulations show an apparent stabilization for shunt impedances above 900 k Ω . The reason for this is that the phase slippage and the consequent tune spread become so large due to the beam loading of the HOM. However, in these simulations, a steady state phase slippage is not reached in 40,000 turns (or even in 100,000 turns, which was also tried) so it cannot be said that the beam is stable.

IV. EXPERIMENT

Following the theoretical and simulation studies outlined in Sec. III, a method was devised to investigate experimentally the dependence of coupled-bunch quadrupole stability on the fill pattern. Because it is not possible to vary the shunt impedance of a HOM in reality, measurements were instead made of the threshold Landau-cavity voltage above which a quadrupole instability appears. It has already been shown that this can act as a proxy measurement of the same thing

since a lower Landau-cavity voltage (higher Landau-cavity detuning) will result in a larger threshold shunt impedance as shown in Fig. 2. Experiments were performed on the MAX IV 3 GeV ring. As in the simulations (Sec. III), a longitudinal feedback is needed to keep the coupled-bunch dipole modes stable. Although some damping of quadrupole modes can be achieved [4], the feedback used [12] is principally designed to damp dipolar bunch motion. It performs phase detection by mixing the sum signal from a four-button rf pick-up with a 600 MHz local oscillator and uses a longitudinal cavity kicker with a resonant frequency of around 625 MHz [13] as an actuator. As an added motivation, the maximum current that can be stably stored in the MAX IV 3 GeV ring when relying on the longitudinal feedback for stability is limited by a coupled-bunch quadrupole instability [5], although higher stable currents can be achieved when relying on Landau damping from the Landau cavities instead [14].

The experimental results are presented here and compared to calculations for the example HOM. Only qualitative agreement is expected since quantitative agreement would require accurate, detailed knowledge of the driving impedance which would be a large effort to obtain, particularly for nonuniform fills where a coupled-bunch mode could be driven over a broad range of frequencies.

The machine parameters during the measurements were the same as those listed in Table I except the beam current is reduced to 160 mA and the rf voltage is increased to 1.314 MV. In this configuration, a coupled-bunch quadrupole instability appears when the total Landau-cavity voltage is sufficiently high. The spectrum of longitudinal beam motion in a uniform fill when the instability is present is shown in Fig. 5. The peak at around 1400 Hz is due to the appearance of the coupled-bunch quadrupole instability. It is found through a modal decomposition of the bunch-by-bunch motion [15] that the coupled-bunch mode number of the quadrupole instability is 138.

It is important to rule out the possibility that the quadrupole instability is being driven by the feedback

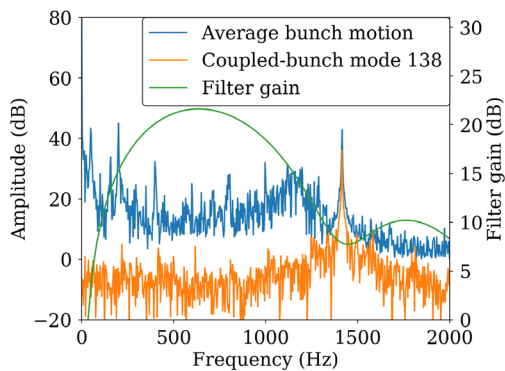


FIG. 5. Beam spectra as measured by the phase detection of the bunch-by-bunch feedback system along with the spectrum of coupled-bunch mode 138 and the frequency response of the FIR filter used in the feedback loop.

itself. The first piece of evidence for this is that the instability appears independent of the FIR filter used in the feedback. To further minimize the influence of the bunch-by-bunch feedback on the instability, a FIR filter is selected that has a notch at the frequency of the quadrupole instability while still being broadband enough to keep the dipole modes stable. The frequency response of the FIR filter is included in Fig. 5.

During the investigation, the vertical channel of the bunch-by-bunch feedback was used to sequentially clean out bunches one by one to vary the fill pattern while frequent injections were made to keep the total beam current constant at 160 mA by increasing the charge stored in the remaining bunches. For each fill pattern, the total Landau-cavity voltage at which the quadrupole instability appeared was recorded. An increased threshold value for the Landau-cavity voltage indicates that the coupled-bunch quadrupole mode is stabilized for that fill pattern.

The results are shown in Fig. 6, along with results calculated for the example HOM, the same machine parameters and the same constant beam current of 160 mA for all fill patterns. For comparison with Fig. 2, the theoretically determined threshold Landau voltage for a uniform fill corresponds to a Landau detuning of 138 kHz. Voltage is used instead of detuning here as it is easier to measure experimentally. It can be said that there is qualitative agreement because the experimental curve shows the same trend as the theoretical curve for the unshifted example HOM. That is, the threshold Landau-cavity voltage increases the fewer the number of filled rf buckets. Both in measurement and in calculation, the threshold voltage appears to saturate below a certain number of filled buckets and then starts to decrease, similar to what is seen in Fig. 3. As mentioned in Sec. III B, due to its dynamic range being limited by its front and back-end frequencies, the bunch-by-bunch feedback becomes less effective as the phase slippage increases. At these Landau-cavity voltages, it is therefore not possible to keep the

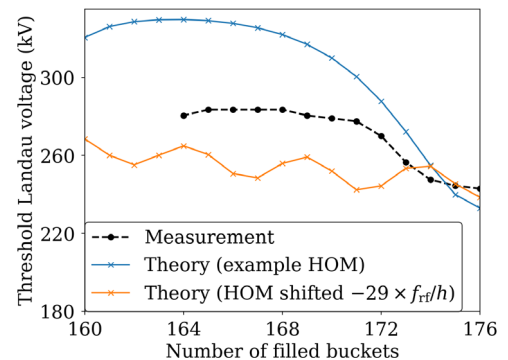


FIG. 6. Threshold Landau-cavity voltage for different fill patterns in the MAX IV 3 GeV ring and calculation of the same for the example HOM and for the HOM shifted in frequency so that it drives coupled-bunch mode 138 when the fill pattern is uniform.

dipole mode stable with fewer than 164 buckets filled so no more points could be measured.

Unlike what might be expected from the macroparticle tracking results shown in Fig. 3, the experimental data does not show any increase in the threshold Landau-cavity voltage for the uniform fill pattern compared to the fill pattern with one bunch removed. However, as pointed out in Sec. III B, in reality the fill pattern will never be completely uniform and there will always be some tune spread between the different bunches. It is therefore not possible to recreate the simulation conditions experimentally and establish definitively what happens when the interbunch tune spread goes to zero.

The theoretical calculation was then repeated with the frequency of the HOM shifted downwards by 29 revolution harmonics so that it drives coupled-bunch mode 138 in a uniform fill, the coupled-bunch mode observed during the experiment. The results for this case are also included in Fig. 6. The curve still shows an overall increase in the threshold Landau-cavity voltage with fewer filled rf buckets but the range of voltages covered by the curve is now greatly reduced. Furthermore, a wave structure is now visible in the curve and it appears to have a period of between 4 and 5 buckets, approximately the same period as the least stable uniform-fill coupled-bunch mode, number 138 ($h/(h - 138) = 4.6$). Further calculations reveal that this is also the case when a different coupled-bunch mode is the least stable. The curve for the unshifted HOM also begins to show a similar structure but the period length is too long to be seen on the figure.

It can be excluded that the cause of the trend observed in experiment is that the HOM is in a Landau cavity and its resonant frequency changes when the Landau-cavities are tuned to adjust the field level, since keeping the detuning fixed when cleaning out one bunch while keeping the current constant results in the quadrupole instability being damped.

The biggest difference between the results of the measurement and of the theoretical calculation for the (unshifted) example HOM is that the latter covers a much larger range of Landau-cavity voltages. In an attempt to determine the reason for this difference, the dependence on the HOM parameters was investigated by performing more calculations. These are summarized in the Appendix, along with an attempt to find parameters of a single HOM that reproduce the measured results.

It is possible, however, that the least stable coupled-bunch quadrupole mode seen in reality is driven across multiple revolution bands by multiple HOMs. There is some evidence for this in the fact that the coupled-bunch mode number observed experimentally with a uniform fill is not the one that is suggested by the shape of the threshold curve. As anticipated, more detailed knowledge of the driving impedance would be desirable for a more quantitative analysis.

V. CONCLUSION

A theory has been developed to evaluate coupled-bunch quadrupole instabilities for arbitrary fill patterns and in the presence of Landau cavities if required. The case of a HOM-driven coupled-bunch quadrupole instability in the MAX IV 3 GeV ring has been investigated. It is found that, particularly for cases with no Landau cavities or a low Landau-cavity voltage, the beam loading of the HOM must be included because the beam phase slippage is greatly affected by a HOM with the threshold shunt impedance for a quadrupole instability. Comparison of theoretical predictions with the results of macroparticle tracking shows good agreement for HOMs close to resonance and over a broad range of Landau-cavity detuning and for different fill patterns.

In general, it is predicted that a nonuniform fill pattern is beneficial for preventing coupled-bunch quadrupole instabilities, i.e., the threshold HOM shunt impedance is greatly increased. Perhaps counterintuitively, it is predicted that the effect is stronger with detuned Landau cavities or no Landau cavities at all. This is because, in this case, the HOM has a large effect on the beam phase slippage and so is self-stabilizing: the higher the HOM shunt impedance, the larger the effect it has on the beam phase slippage and more Landau damping it introduces to prevent an instability. With tuned-in Landau cavities, the incoherent synchrotron tune is lower (increasing the growth rates of coupled-bunch modes) and Landau cavities have a dominant effect over the HOM in terms of inhomogeneous beam loading.

An experiment was performed at the MAX IV 3 GeV ring to further investigate the effect of the fill pattern on the stability of coupled-bunch quadrupole modes. It was found that reducing the number of filled rf buckets improves the stability up to a certain point dependent on the coupled-bunch mode number. This observation will be an important consideration in the development of the alternative delivery configuration for the 3 GeV ring that makes use of the longitudinal bunch-by-bunch feedback and that is employed in case the Landau cavities have to be parked because of technical problems. Qualitative agreement was found with predictions made using the theory, a more complete impedance model being required for quantitative predictions. The theory could therefore be used for the design and development of storage rings where a longitudinal feedback is relied upon for stability since their performance can be limited by coupled-bunch quadrupole modes that the feedback system may not be designed to damp.

ACKNOWLEDGMENTS

The authors would like to thank the members of the Accelerator Operations group at MAX IV for their invaluable support during the experiments. The MBTRACK

simulations were carried out on the MAX IV computing cluster, for which we thank the members of the Controls and IT group.

APPENDIX: HOM PARAMETER DEPENDENCE

As discussed in Sec. IV, qualitative agreement between theoretical calculations and the results of beam measurements has been achieved. Quantitative agreement would require knowledge of the driving impedance which comes from cavity HOMs. With the aim of understanding what kind of impedance would produce the experimental results, further calculations were done to determine the dependence of the theoretical results on the HOM parameters, specifically the shunt impedance, quality factor and the frequency offset from resonance. While by no means exhaustive, this investigation should improve understanding of the experimental results. The effect of shifting the HOM by a multiple of the revolution frequency is discussed in Sec. IV while moving the HOM by an exact multiple of the rf frequency should not make much difference except for the fact that the bunch form factors would be different.

The trend to be interpreted is the effect of the fill pattern on the threshold Landau-cavity voltage for a coupled-bunch quadrupole instability. Figure 7 shows the effect of varying the shunt impedance and quality factor of the HOM. It can be seen that the main effect of increasing the shunt impedance is to move the curve to lower Landau-cavity voltages. This confirms that measuring the threshold Landau-cavity voltage is a good proxy for measurement of the threshold shunt impedance. However, it does also slightly change the range of Landau-cavity voltages covered by the curve. The effect of varying the quality factor is very small in this regime because the HOM is on resonance and in all cases, the damping time of the HOM is very large in comparison to the time interval between bunches.

The effect of changing the frequency offset of the HOM is shown in Fig. 8. Small frequency shifts are chosen so the

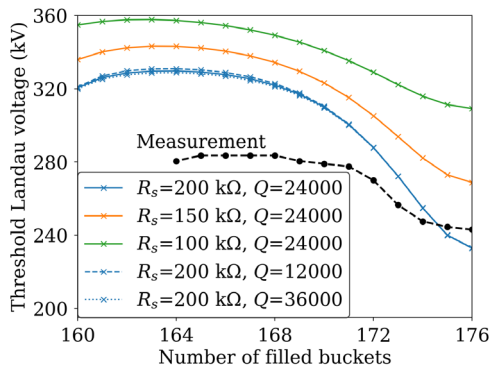


FIG. 7. Threshold Landau-cavity voltage for different fill patterns in the MAX IV 3 GeV as calculated for different HOM shunt impedances and quality factors. The measured curve is also included for reference.

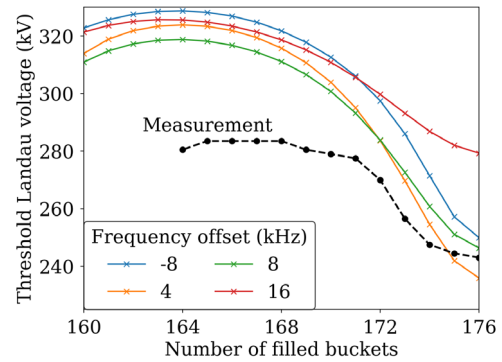


FIG. 8. Threshold Landau-cavity voltage for different fill patterns in the MAX IV 3 GeV as calculated for different frequency offsets of the HOM from resonance. The measured curve is also included for reference.

effect is mostly in the shape of the curve rather than the mean value. It can be seen that a positive frequency offset does result in quite a significant reduction in the range of the curve without affecting the mean value as much as the shunt impedance does.

Finally, an attempt was made to find the parameters of a single HOM that best reproduce the measured curve. This was based on the following methodology. First, the location of the peak in the curve was matched by scanning the revolution harmonic of the HOM. This parameter could then be fixed as it is discrete in nature and relatively independent of the other HOM parameters. Next, a combination of HOM detuning and quality factor was found that approximately reproduces the range of the measured curve. Finally, the shunt impedance was scanned to match the mean value. Further adjustments to the quality factor were made but these had a small effect. The results are shown in Fig. 9. Errors on the measured data points have been estimated as a scale-reading error of 0.75 kV, since the Landau-cavity voltage was increased in steps of 1.5 kV until the threshold where the beam went unstable was found. This step size was limited by the feedback acting on the measured Landau-cavity field and is clearly small

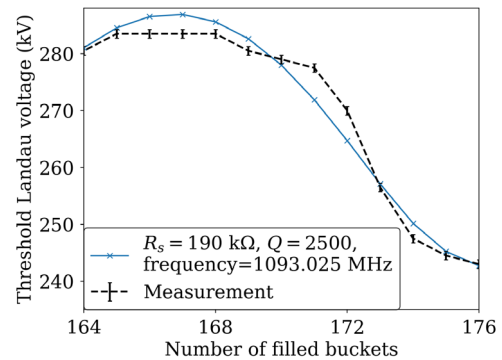


FIG. 9. Threshold Landau-cavity voltage for different fill patterns in the MAX IV 3 GeV as calculated for HOM parameters chosen to reproduce the measured curve.

enough. It can be seen that with the specific HOM parameters found, the theoretical curve reproduces the measured one reasonably well and achieves a lower residual sum of squares than a third-order polynomial fit, which has the same number of parameters. However, it cannot be said that there is agreement between the two curves to within the experimental uncertainties.

-
- [1] F. J. Cullinan, Å. Andersson, and P. F. Tavares, Harmonic-cavity stabilization of longitudinal coupled-bunch instabilities with a nonuniform fill, *Phys. Rev. Accel. Beams* **23**, 074402 (2020).
- [2] T. Olsson, F. J. Cullinan, and Å. Andersson, Self-consistent calculation of transient beam loading in electron storage rings with passive harmonic cavities, *Phys. Rev. Accel. Beams* **21**, 120701 (2018).
- [3] R. Warnock and M. Venturini, Equilibrium of an arbitrary bunch train in presence of a passive harmonic cavity: Solution through coupled Haïssinski equations, *Phys. Rev. Accel. Beams* **23**, 064403 (2020).
- [4] A. Drago, A. Gallo, A. Ghigo, M. Zobov, J. D. Fox, and D. Teytelman, Longitudinal quadrupole instability and control in the Frascati daΦne electron ring, *Phys. Rev. ST Accel. Beams* **6**, 052801 (2003).
- [5] F. J. Cullinan, Feedbacks against collective instabilities at MAX IV. 11 2018, *Presented at the Joint ARIES Workshop on Electron and Hadron Synchrotrons*, https://indico.cern.ch/event/743699/contributions/3112143/attachments/1750504/2840093/Cullinan_ARIESfbwkshpNov18.pdf.
- [6] G. Skripka, R. Nagaoka, M. Klein, F. Cullinan, and P. F. Tavares, Simultaneous computation of intrabunch and interbunch collective beam motions in storage rings, *Nucl. Instrum. Methods Phys. Res., Sect. A* **806**, 221 (2016).
- [7] R. R. Lindberg, Theory of coupled-bunch longitudinal instabilities in a storage ring for arbitrary rf potentials, *Phys. Rev. Accel. Beams* **21**, 124402 (2018).
- [8] M. Venturini, Passive higher-harmonic rf cavities with general settings and multibunch instabilities in electron storage rings, *Phys. Rev. Accel. Beams* **21**, 114404 (2018).
- [9] R. A. Bosch, K. J. Kleman, and J. J. Bisognano, Robinson instabilities with a higher-harmonic cavity, *Phys. Rev. ST Accel. Beams*, **4**, 074401 (2001).
- [10] T. Suzuki, Theory of longitudinal bunched beam instabilities based on the Fokker-Planck equation, *Part. Accel.* **14**, 91 (1983), <https://inspirehep.net/files/f0fa0c5c7e0371e449f62d99a090dfb4>.
- [11] D. Teytelman, Coupled-bunch Instabilities and the Anna Karenina Principle, *Presented at the Joint ARIES Workshop on Electron and Hadron Synchrotrons, 2018*, https://indico.cern.ch/event/743699/contributions/3112116/attachments/1752476/2840051/dt_feedback_aries_20181114.pdf.
- [12] Dimtel Inc., URL <https://www.dimtel.com>.
- [13] D. Olsson, L. Malmgren, and K. Ahnberg, A waveguide overloaded cavity kicker for the MAX IV bunch-by-bunch feedback system, in *8th International Particle Accelerator Conference (JACoW, Geneva, 2017)*.
- [14] Å. Andersson, *Status of the MAX IV storage rings, 2019, Presented at ESLS XXVII*, https://indico.cells.es/event/224/contributions/882/attachments/721/1093/AA_Status_MAXIV_v3.pdf.
- [15] S. Prabhakar, J. D. Fox, D. Teytelman, and A. Young, Phase space tracking of coupled-bunch instabilities, *Phys. Rev. ST Accel. Beams* **2**, 084401 (1999).